

The surge-like eruption of a miniature filament associated with circular flare ribbon

Haidong Li^{1,2,3} · Jiayan Yang^{1,2} · Yunchun Jiang^{1,2} · Yi Bi^{1,2,3} · Zhining Qu⁴ · Hechao Chen^{1,2,3}

Received: 7 May 2017 / Accepted: 27 December 2017 / Published online: 4 January 2018
© Springer Science+Business Media B.V., part of Springer Nature 2018

Abstract We present a study of a mini-filament erupting in association with a circular ribbon flare observed by NVST and SDO/AIA on 2014 March 17. The filament was located at one footpoint region of a large loops. The potential field extrapolation shows that it was embedded under a magnetic null point configuration. First, we observed a brightening of the filament at the corresponding EUV images, close to one end of the filament. With time evolution, a circular flare ribbon was observed around the filament at the onset of the eruption, which is regarded as a signature of reconnection at the null point. After the filament activation, its eruption took the form of a surge, which ejected along one end of a large-scale closed coronal loops with a curtain-like shape. We conjecture that the null point reconnection may facilitate the eruption of the filament.

Keywords Sun: activity · Sun: filaments, prominences · Sun: corona · Sun: magnetic fields · Sun: flares · Sun: magnetic topology

Electronic supplementary material The online version of this article (<https://doi.org/10.1007/s10509-017-3244-3>) contains supplementary material, which is available to authorized users.

✉ H. Li
lhd@ynao.ac.cn

- ¹ Yunnan Observatories, Chinese Academy of Sciences, 396 Yangfangwang, Guandu District, Kunming, 650216, China
- ² Center for Astronomical Mega-Science, Chinese Academy of Sciences, 20A Datun Road, Chaoyang District, Beijing, 100012, China
- ³ University of Chinese Academy of Sciences, Beijing 100049, China
- ⁴ Department of Physics, School of Science, Sichuan University of Science and Engineering, Zigong 643000, China

1 Introduction

Mini-filament eruptions are common activity phenomena occurring everywhere on the Sun. Along magnetic polarity inversion lines (PILs), miniature filaments show a curved shape, and their eruptions are usually associated with magnetic flux emergence and cancellation in the photosphere (Wang et al. 2000; Hong et al. 2011). Similar to large-scale filament eruptions, the miniature filament eruptions are often accompanied by two-ribbon flares (e.g., Liu et al. 2010).

In a complicated fan spine configuration, moreover, small-scale filament eruption is associated with a null point reconnection, producing a circular ribbon (Wang and Liu 2012; Liu et al. 2015; Li et al. 2017b; Zhang et al. 2015; Hong et al. 2017). Under such configuration, the activation and rising of the filament usually disturb the null point, and even interact with the field near the null point (Liu et al. 2015; Li et al. 2017b). On the other hand, some authors even speculated that the null point reconnection may facilitate the filament eruption (Jiang et al. 2013; Sun et al. 2013). The null-point reconnection in this setting is likely of the “breakout” nature (Antiochos 1998; Antiochos et al. 1999; Shen et al. 2012a). In a multipolar system the reconnection process, involved weaker overlying field, is generally mild, but is crucial to the subsequent eruptions. This process may alleviate the constraints on the filament and reduce the magnetic tension force that stabilizes the system, then less energy is required to open the higher-lying loops. Simulations of blowout of the twisted jet core field by the breakout reconnection with ambient fields were also conducted (Pariat et al. 2009; Rachmeler et al. 2010). Rachmeler et al. (2010) suggested that reconnection is indeed necessary for jet formation in symmetric jet models in a uniform coronal background field.

When the null point reconnection occurs, energized and accelerated particles flow down from the reconnection site

along the magnetic field line propagate toward footpoint, precipitating at different layers of the solar atmosphere (Priest and Forbes 2002). The produced emissions are observed in both the photosphere and the corona, appeared as circular ribbon, which exactly matches the footpoints of the fan field lines (Reid et al. 2012; Wang and Liu 2012; Sun et al. 2013; Yang et al. 2015a). For the complicated magnetic topology, many studies have shown that magnetic reconnection favorable occurs at quasi-separatrix layers (QSLs) (Milano et al. 1999; Aulanier et al. 2005; Lawrence and Gekelman 2009; Wilmot-Smith et al. 2010; Gekelman et al. 2012), which divides domains of distinct connectivity with strong connectivity gradients (Mandrini et al. 1991; Demoulin et al. 1997). Through calculate the squashing factor, the gradient of the field line linkage can be measured (Titov et al. 2002).

To our knowledge, filament eruptions of chromosphere may play a key role in the formation of jets or surges (Shen et al. 2012b; Sterling et al. 2015; Hong et al. 2016, 2017; Li et al. 2017b). Especially, there are few reports about the observation of miniature filament eruption under a null point magnetic topology. The null point reconnection of the jets is apparently analogous to the breakout process involved in the production of major coronal mass ejections (CMEs) (Antiochos et al. 1999). The filament eruption associated with circular ribbon provides direct support for the model of Moore et al. (2010), which depicts a jet-scale magnetic breakout. Therefore, the kinematics of a small-scale filament eruption associated with a surge are desired in order to further understand the physics of the jet phenomenon.

2 Data calibration, alignment, and magnetic field modeling

For this study, we mainly used multi-wavelength data from the Atmospheric Imaging Assembly (AIA; Lemen et al. 2012) and the Helioseismic and Magnetic Imager (HMI; Schou et al. 2012) on board the *Solar Dynamics Observatory* (SDO; Pesnell et al. 2012) and ground-based $H\alpha$ observations of the New Vacuum Solar Telescope (NVST; Liu and Beckers 2001; Liu et al. 2014). Observations from both SDO/AIA and NVST provided a good opportunity to study the eruption of a filament phenomenon and associated circular flare ribbon. A $H\alpha$ channel high resolution imaging system of NVST can be used to observe the fine structures in the chromosphere. The $H\alpha$ filter was a tunable Lyot filter with a bandwidth of 0.25 \AA . It can scan spectra in the $\pm 5 \text{ \AA}$ range with a step size of 0.1 \AA . We examined $H\alpha$ 6162.8 \AA images that obtained by NVST from 05:47 UT to 09:34 UT on 2014 March 17. The high-resolution data was very suitable to trace the erupting process of mini-filament with a spatial resolution of $0.32''$ at a cadence of 12 s. The calibrated Level 1+ data underwent a flat-field-correction and

dark-current-subtraction with the speckle masking method (Weigelt 1977). The method of the high-resolution reconstruction of NVST data was described in detail by Xiang et al. (2016). All of $H\alpha$ images were further co-aligned based on a subpixel level image registration procedure (Feng et al. 2012; Yang et al. 2015b). Recently, several works have been published using NVST data (Bi et al. 2015; Li et al. 2015b; Hong et al. 2016, 2017; Shen et al. 2015, 2017; Xue et al. 2016; Yan et al. 2015; Yang et al. 2014, 2015c, 2017; Wang et al. 2016; Tian et al. 2017).

To better understand the magnetic field configuration within the filament's eruption region, we used the Fourier transform method (Alissandrakis 1981) to derive potential field extrapolation by using the vector magnetic field data (HMI; Schou et al. 2012). We also calculated squashing factor Q by using the code induced by Liu et al. (2016). The squashing factor associated with the field lines is defined as $\text{slog } Q \equiv \text{sign}(B_z) \times \log_{10} Q$ (Titov et al. 2011).

3 Results

The surge was originated from the northwest part of AR 12002 ($S20^\circ W40^\circ$) on 2014 March 17. Figure 1 shows the

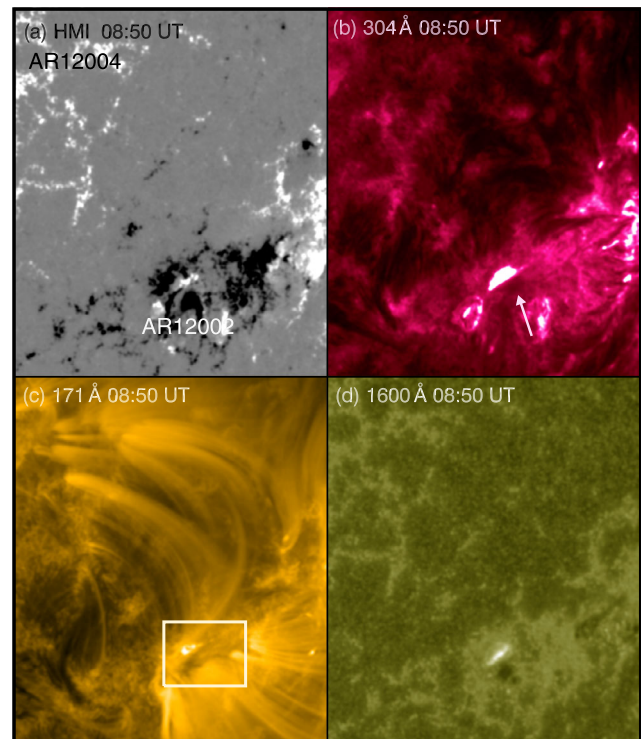
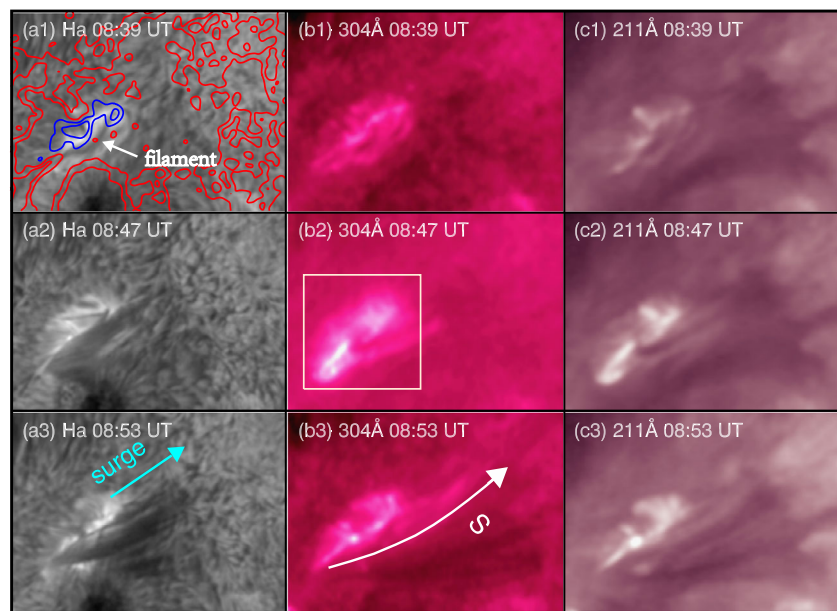


Fig. 1 (a) HMI magnetogram, (b) AIA 304 \AA image showing the erupting surge (indicated by the arrow), (c) AIA 171 \AA image showing large-scale coronal loops that linked ARs 12002 and 12004, and (d) AIA 1600 \AA image showing the brightening of surge footpoint in the chromosphere. The white box in (c) indicates the field of view (FOV) in Fig. 2. The FOV is $230'' \times 270''$

Fig. 2 NVST $H\alpha$, AIA 304 and 211 Å images show the eruption of the surge. The simultaneous HMI magnetogram is overplotted as the *blue/red contours* for positive/negative polarity in panel (a), with contour levels of 100, 290, -100, and -290 G. The *white box* in panel (b2) indicates the FOV in Fig. 4, in which the light curves are measured as shown in Fig. 3(a). The *curved arrow*, “S”, marks the slit position of the time slice shown in Fig. 3(b)–(d). The FOV is $55'' \times 40''$



general appearance of the AR and the occurring surge in AIA 304 Å and 171 Å. Clearly, the surge base appeared as a transient brightening in 1600 Å image (panel (d)) and corresponds to the southern footpoint region of a large-scale coronal loops system connecting AR 12002 to 12004 ($S10^{\circ}W30^{\circ}$), and the 304 Å and 171 Å images (panels (b) and (c)) show that the surge was ejected along the southern legs of the large-scale coronal loops.

Figure 2 shows the eruption of the filament and the formation of the surge in multiwavelength observations obtained by the NVST and SDO/AIA. Thanks to the high-resolution $H\alpha$ line-center observations, we can identify that there exists a tiny filament before the surge’s formation (panel (a1)). To aid matching, HMI magnetograms shows the simultaneous photospheric magnetic field below filament (see panel (a)). The filament sited above the polarity inversion between opposite polarities. It has a projected length about 1.88×10^4 km, which corresponds to the length of miniature filaments observed by Wang et al. (2000).

The evolution of surge was displayed in $H\alpha$, AIA 304 and 211 Å wavebands. At 08:47 UT, one end of the filament began to rise, accompanying with a bright patch around the filament (see panel (b2 and c2)). In this process, the filament erupted as a surge, which showed up as slightly curved and extended linear structures (panel (a3, b3 and c3)), with much size than that of its footpoint bright patch. At 08:53 UT, EUV surge expanded to its maximum length (see panel (b3 and c3)). At the $H\alpha$ images, the ejection plasma showed more slender shape compared to the surge at 304 and 211 Å. Two accompanying animations at EUV and $H\alpha$ can be provided to depict the behavior in more detail.

To study filament material dynamics and multi-thermal structures more clearly after eruption, time slices along a

slit, “S”, indicated by the longer arrow in Fig. 3, are constructed from AIA 304, 211, and 131 Å images. The result is given in Fig. 3(b)–(e), in which the ejecting material appeared as a parabolic bright (dark) streak. We note that the surge ejected at a projected speeds range from 117 km s^{-1} to 147 km s^{-1} with brightening trajectories of the material. After 08:55 UT, these material appeared falling back, the acceleration of material flows is about $0.13\text{--}0.14 \text{ km s}^{-2}$, which is less than the solar gravitational acceleration (0.27 km s^{-2}). In our case, the accelerated speed is similar to the results of Shen et al. (2011) and Roy (1973) that the acceleration of falling material in $H\alpha$ surges and EUV jets being less than free fall. The obtained value is only a fraction of free fall. This apparent discrepancy is possibly results from the projection or the damping effects of the magnetized plasmas in coronal loops. Based on the ratio of the acceleration of falling material along the surge’s axis to the free fall acceleration, we can estimate the angle of the ejective surge with the plane of the sky that is about 60° .

Before filament eruption some brightenings appeared at the bottom of the time-slices, implying that there are some reconnection process happened before the formation of the surge, which may remove the field line above the filament (Fig. 3(b)–(e)). We note that a brightening occurred at 131 Å image at 08:43 UT (see Fig. 4(b)), which corresponds to one end of the filament. Soon afterward, at 08:44 UT, a circular brightening formed in 131 Å above PIL between the central positive field and the surrounding negative field (Fig. 4(d)). As the global filament appeared as a long strip of brightness and became active, the circular brightening also formed completely (Fig. 4(e)–(f)). What type of coronal magnetic field topology will lead to the observed circular flare ribbon? As we known, the null point reconnection is often associated

Fig. 3 Panel (a) shows the positive (pink solid line) and the negative (pink dashed line) magnetic fluxes of the surge's base region as shown in Fig. 4 during the surge eruption period. It also shows the light curves of the same region in AIA 94, 131, 211, 1600 Å, and NVST H α passbands indicated by green, dark green, magenta, olive, and black lines. The red, green, and blue arrows emphasize the first, second, and third peaks, respectively. Panels (b)–(d) show time-distance diagrams obtained from 304, 211, and 131 Å, along S with a width of 3'' (indicated in Fig. 2(b3)). The straight dotted lines are linear fit to the bright stripes, and the curves are least-squares polynomial fits to the falling plasmas

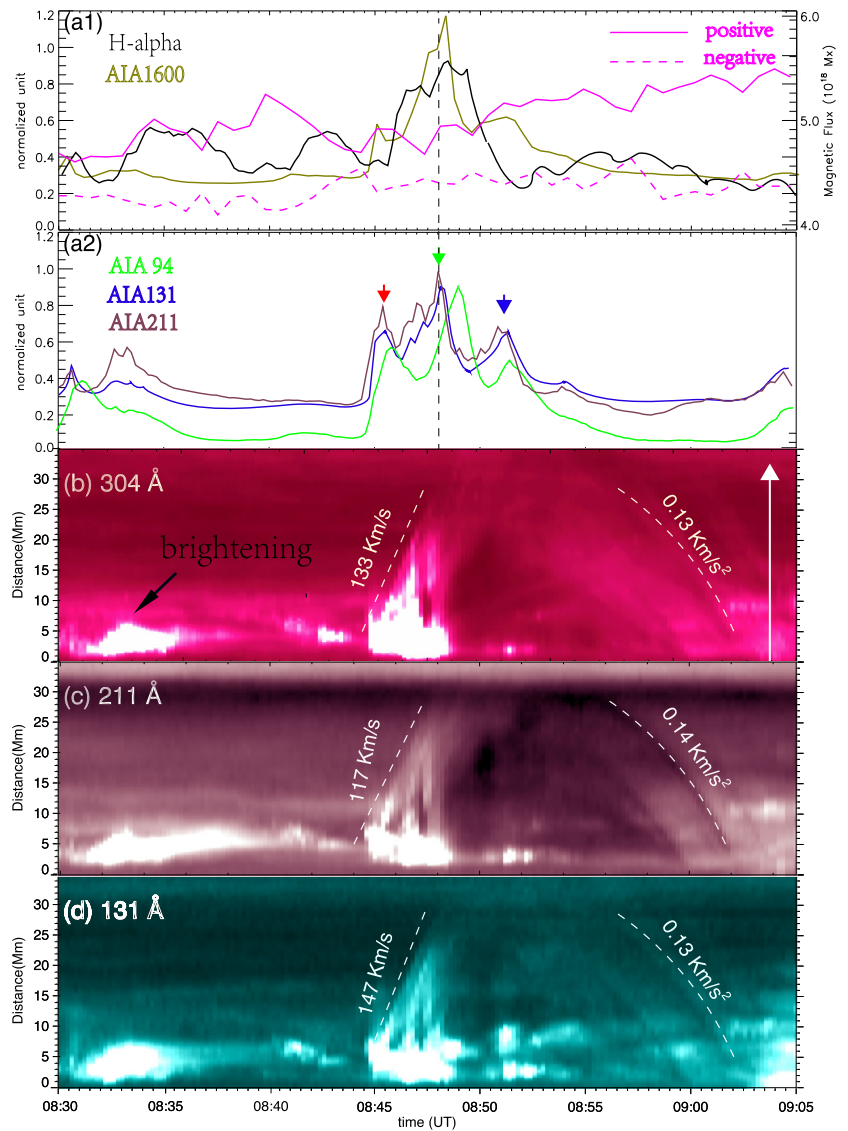
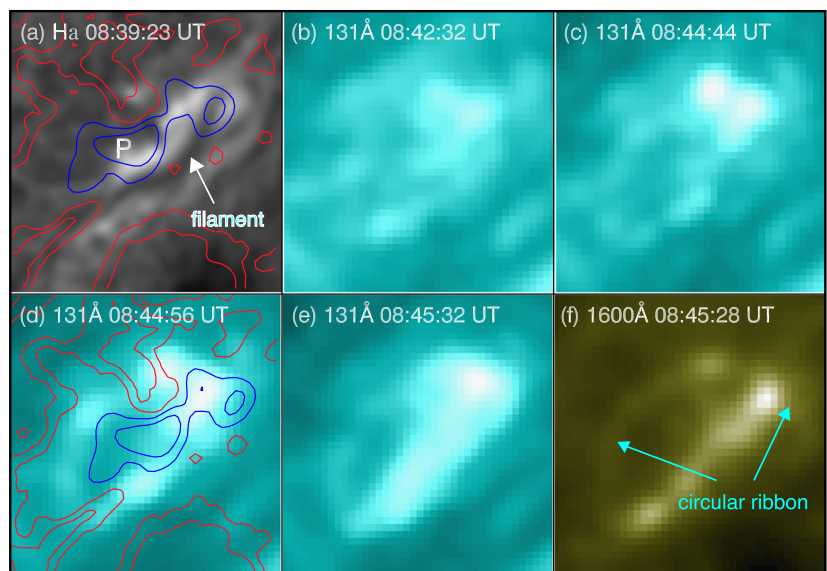


Fig. 4 Panels (a)–(e) are NVST H α , AIA 131, and 1600 Å images, showing the morphological feature of the filament before the eruption and the evolution of circular ribbon flare. The simultaneous HMI magnetogram is overplotted as the blue/red contours for positive/negative polarity in panels (a) and (d), with contour levels of 100, 290, –100, and –290 G. The FOV is 24'' \times 24''



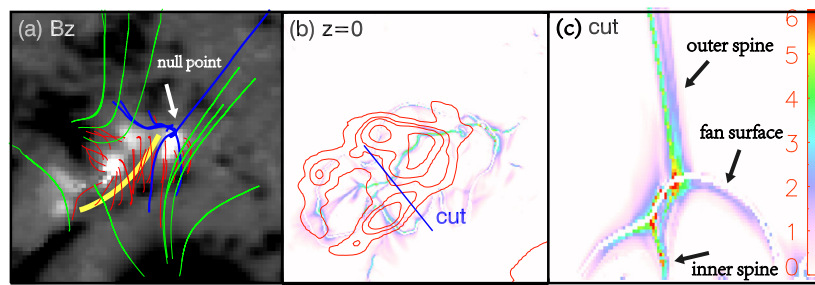


Fig. 5 (a) The background shows the photospheric vertical magnetic field. Magnetic field around the filament at 08:48 UT is calculated from a potential coronal field extrapolation. The closed coronal loops are depicted by *red lines*, and parts of them located above the filament (*yellow line*). The *green field lines* is open field lines relative to small closed coronal loops. In particular, the null point indicated by *white*

arrow is a site where magnetic field lines converge. (b) Map of the squashing factor Q in the x - y plane at $z = 0$. The intensity of 1600 Å image at 08:48 UT is overplotted on it as the *red contours*. (c) The corresponding vertical cross-section of Q in a plane are indicated by a solid line in panel (b)

with circular ribbon flare. The remarkably circular ribbon strongly confirmed the present of a magnetic null configuration. For the region of the filament eruption, a positive polarity was surrounded by negative polarity. This feature implies the existence of a magnetic null point in the corona (Antiochos 1998). Using the trilinear null finding method (Haynes and Parnell 2007), we detected a coronal null point that suited at 3 Mm height above the western part of positive magnetic pole (Fig. 5(a)). The potential field extrapolation revealed the magnetic field configuration of the filament (Fig. 5(a)), which is similar to previous proposed fan spine magnetic topology (Masson et al. 2009; Wang and Liu 2012).

The magnetic fluxes of the surge footpoint region and the light curve of the same region are measured from continuous observations. These results are given in Fig. 3(a). There is no significant evolution relation between the positive/negative magnetic flux and the filament eruption. The light curves in NVST H α , AIA 94, 131, 211, and 1600 Å displayed obvious emission enhancement. The light curves of AIA 94, 131, and 211 Å consisted of three main peaks. The first peak at 08:45 UT indicated by red arrow corresponds to the brightening of circular ribbon generated by reconnection of the null point. The circular brightening can be observed at 131 Å images (08:45 UT) as shown in Fig. 5(d) and (e). The second peak (the strongest value) may be caused by internal reconnection, among the legs of the erupting filament. However, for the limitation of observational capability, there is no appreciable resolution to identify a two ribbon flare in the base. About the third peak, however, we can only give an ambiguous interpretation that the brightening is originated from a recurrent magnetic reconnection of the surge base (Li et al. 2015a). Moreover, the light curve in H α and AIA 1600 Å showing only one main peak implies that in the chromosphere the circular ribbon was not obvious before the eruption.

Using the code induced by Liu et al. (2016), we calculated the QSLs derived from a potential field extrapolation to

emphasize some of the identified QSL structure. In Fig. 5(b), the distribution of the squashing factor Q in the x - y plane for $z = 0$ was displayed clearly. To get the relation between the flare ribbon and topology structure, the intensity of AIA 1600 Å image was overplotted on the Q map. The region with strong values in the Q map not match well circular ribbon in AIA 1600 Å. This may imply that the null point topology structure is a very complicated structure. We also plot the distribution of the squashing factor in plane that perpendicular to the x - y plane (marked in panel (b)). It is seen that multiple QSLs tend to converge and intersect at the height of the null point above photosphere, implying this eruption occurred under a fine spine configuration (panel (c)).

4 Conclusions

By means of observations from NVST and SDO/AIA, the event was identified as a mini-filament eruption taking place in the form of a surge, which was located at a footpoint of large-scale coronal loop. The main results are summarized as follows:

1. A notable feature of this event is that the circular ribbon surrounding the filament, accompanied with an eruption of filament. The presence of the circular ribbon implies a configuration favorable for coronal point null reconnection to occur. Data observations and a potential field extrapolation imply that the circular flare ribbon result from null point reconnection of the coronal magnetic field. The energetic electrons generated by null point reconnection were accelerated and spiral downward along the fan-like field lines to the intersection of the fan with the photosphere.

2. The eruptive event is also like several authors reported filament/flux rope eruption under fan spine structure, which produced circular flare ribbon in association with null point reconnection (Wang and Liu 2012; Sun et al. 2013; Jiang et al. 2013; Joshi et al. 2015; Liu et al. 2015; Yang et al.

2015a; Li et al. 2017a,b; Hong et al. 2017; Xu et al. 2017). In a magnetic topology contained a null point, Jiang et al. (2013) reported that a circular flare ribbon occurred a little earlier than the rising of the flux rope. They suggest that the null point reconnection may cut the overlying field lines and facilitate the outward expansion of the flux rope. In the study of homologous circular-ribbon flares, Xu et al. (2017) suggested that continuous input of the free energy in the form of a flux rope from beneath the photosphere may drive a breakout-type reconnection occurring high in the corona, which could release the constraint on the flux rope and trigger the MHD instability to make filament lose equilibrium. In our case, the activity of the filament is associated with the brightening of the circular ribbon. We conjecture that the null point reconnection may facilitate the eruption of the filament.

3. Previous studies have shown that many small-scale filament eruptions usually take the shape of coronal jets (Yang et al. 2012; Li et al. 2017b). They were found to associate with cancellations and convergences of opposite fluxes, and the ejective material propagated along the closed coronal loops. In our case, the filament eruption is also confined by the coronal loops, so the plasma can not escape to the outerspace.

Acknowledgements We thank an anonymous referee for providing detailed suggestions and comments that significantly improved the presentation of this paper. We are grateful to the NVST, AIA, and HMI teams for data support. This work is supported by the National Natural Science Foundation of China under grants 11633008, 11333007, 11703084, 11503081, 11573012, and 11503082, by the CAS programs “Light of West China” and “QYZDJ-SSW-SLH012”, by Foundation of Sichuan University of Science and Engineering grant 2015RC43, and by the grant associated with the Project of the Group for Innovation of Yunnan Province.

References

- Alissandrakis, C.E.: *Astron. Astrophys.* **100**, 197 (1981)
 Antiochos, S.K.: *Astrophys. J.* **502**, L181 (1998)
 Antiochos, S.K., DeVore, C.R., Klimchuk, J.A.: *Astrophys. J.* **510**, 485 (1999)
 Aulanier, G., Parlat, E., D emoulin, P.: *Astron. Astrophys.* **444**, 961 (2005)
 Bi, Y., Jiang, Y., Yang, J., et al.: *Astrophys. J.* **805**, 48 (2015)
 Demoulin, P., Bagala, L.G., Mandrini, C.H., Henoux, J.C., Rovira, M.G.: *Astron. Astrophys.* **325**, 305 (1997)
 Feng, S., Deng, L., Shu, G., et al.: *Advanced Computational Intelligence (ICACI)*. In: 2012 IEEE Fifth International Conference, p. 626 (2012)
 Gekelman, W., Lawrence, E., Van Compernelle, B.: *Astrophys. J.* **753**, 131 (2012)
 Haynes, A.L., Parnell, C.E.: *Phys. Plasmas* **14**, 082107 (2007)
 Hong, J., Jiang, Y., Zheng, R., et al.: *Astrophys. J. Lett.* **738**, L20 (2011)
 Hong, J., Jiang, Y., Yang, J., et al.: *Astrophys. J.* **830**, 60 (2016)
 Hong, J., Jiang, Y., Yang, J., et al.: *Astrophys. J.* **835**, 35 (2017)
 Jiang, C., Feng, X., Wu, S.T., Hu, Q.: *Astrophys. J. Lett.* **771**, L30 (2013)
 Joshi, N.C., Liu, C., Sun, X., et al.: *Astrophys. J.* **812**, 50 (2015)
 Lawrence, E.E., Gekelman, W.: *Phys. Rev. Lett.* **103**, 105002 (2009)
 Lemen, J.R., Title, A.M., Akin, D.J., et al.: *Sol. Phys.* **275**, 17 (2012)
 Li, H., Jiang, Y., Yang, J., et al.: *Astrophys. Space Sci.* **359**, 4 (2015a)
 Li, X., Yang, S., Chen, H., Li, T., Zhang, J.: *Astrophys. J. Lett.* **814**, L13 (2015b)
 Li, H., Jiang, Y., Yang, J., et al.: *Astrophys. J.* **836**, 235 (2017a)
 Li, H., Jiang, Y., Yang, J., et al.: *Astrophys. J. Lett.* **842**, L20 (2017b)
 Liu, Z., Beckers, J.M.: *Sol. Phys.* **198**, 197 (2001)
 Liu, C., Lee, J., Jing, J., et al.: *Astrophys. J. Lett.* **721**, L193 (2010)
 Liu, Z., Xu, J., Gu, B., et al.: *Res. Astron. Astrophys.* **14**, 705 (2014)
 Liu, C., Deng, N., Liu, R., et al.: *Astrophys. J. Lett.* **812**, L19 (2015)
 Liu, R., Kliem, B., Titov, V.S., Chen, J., Wang, Y., Wang, H., Liu, C., Xu, Y., Wiegmann, T.: *Astrophys. J.* **818**, 148 (2016)
 Mandrini, C.H., Demoulin, P., Henoux, J.C., Machado, M.E.: *Astron. Astrophys.* **250**, 541 (1991)
 Masson, S., Parlat, E., Aulanier, G., Schrijver, C.J.: *Astrophys. J.* **700**, 559 (2009)
 Milano, L.J., Dmitruk, P., Mandrini, C.H., G omez, D.O., D emoulin, P.: *Astrophys. J.* **521**, 889 (1999)
 Moore, R.L., Cirtain, J.W., Sterling, A.C., Falconer, D.A.: *Astrophys. J.* **720**, 757 (2010)
 Parlat, E., Antiochos, S.K., DeVore, C.R.: *Astrophys. J.* **691**, 61 (2009)
 Pesnell, W.D., Thompson, B.J., Chamberlin, P.C.: *Sol. Phys.* **275**, 3 (2012)
 Priest, E.R., Forbes, T.G.: *Astron. Astrophys.* **10**, 313 (2002)
 Rachmeler, L.A., Parlat, E., DeForest, C.E., Antiochos, S., Torok, T.: *Astrophys. J.* **715**, 1556 (2010)
 Reid, H.A.S., Vilmer, N., Aulanier, G., Parlat, E.: *Astron. Astrophys.* **547**, A52 (2012)
 Roy, J.R.: *Sol. Phys.* **32**, 139 (1973)
 Schou, J., Scherrer, P.H., Bush, R.I., et al.: *Sol. Phys.* **275**, 229 (2012)
 Shen, Y., Liu, Y., Su, J., Ibrahim, A.: *Astrophys. J.* **735**, L43 (2011)
 Shen, Y., Liu, Y., Su, J.: *Astrophys. J.* **750**, 12 (2012a)
 Shen, Y., Liu, Y., Su, J., Deng, Y.: *Astrophys. J.* **745**, 164 (2012b)
 Shen, Y., Liu, Y., Liu, Y.D., et al.: *Astrophys. J. Lett.* **814**, L17 (2015)
 Shen, Y., Liu, Y.D., Su, J., Qu, Z., Tian, Z.: *Astrophys. J.* **851**, 67 (2017)
 Sterling, A.C., Moore, R.L., Falconer, D.A., Adams, M.: *Nature* **523**, 437 (2015)
 Sun, X., Hoeksema, J.T., Liu, Y., et al.: *Astrophys. J.* **778**, 139 (2013)
 Tian, Z., Liu, Y., Shen, Y., et al.: *Astrophys. J.* **845**, 94 (2017)
 Titov, V.S., Hornig, G., D emoulin, P.: *J. Geophys. Res. Space Phys.* **107**, 1164 (2002)
 Titov, V.S., Miki, Z., Linker, J.A., Lionello, R., Antiochos, S.K.: *Astrophys. J.* **731**, 111 (2011)
 Wang, H., Liu, C.: *Astrophys. J.* **760**, 101 (2012)
 Wang, J., Li, W., Denker, C., et al.: *Astrophys. J.* **530**, 1071 (2000)
 Wang, J., Yan, X., Qu, Z., et al.: *Astrophys. J.* **817**, 156 (2016)
 Weigelt, G.P.: *Opt. Commun.* **21**, 55 (1977)
 Wilmot-Smith, A.L., Pontin, D.I., Hornig, G.: *Astron. Astrophys.* **516**, A5 (2010)
 Xiang, Y-y., Liu, Z., Jin, Z-y.: *New Astron.* **49**, 8 (2016)
 Xu, Z., Yang, K., Guo, Y., et al.: *Astrophys. J.* **851**, 30 (2017)
 Xue, Z., Yan, X., Cheng, X., et al.: *Nat. Commun.* **7**, 11837 (2016)
 Yan, X.L., Xue, Z.K., Pan, G.M., et al.: *Astrophys. J. Suppl. Ser.* **219**, 17 (2015)
 Yang, J., Jiang, Y., Yang, B., et al.: *New Astron.* **17**, 732 (2012)
 Yang, S., Zhang, J., Xiang, Y.: *Astrophys. J. Lett.* **793**, L28 (2014)
 Yang, K., Guo, Y., Ding, M.D.: *Astrophys. J.* **806**, 171 (2015a)
 Yang, Y-F., Qu, H-X., Ji, K-F., et al.: *Res. Astron. Astrophys.* **15**, 569 (2015b)
 Yang, S., Zhang, J., Xiang, Y.: *Astrophys. J. Lett.* **798**, L11 (2015c)
 Yang, L., Yan, X., Li, T., et al.: *Astrophys. J.* **838**, 131 (2017)
 Zhang, Q.M., Ning, Z.J., Guo, Y., et al.: *Astrophys. J.* **805**, 4 (2015)